ISSN 1070-4272, Russian Journal of Applied Chemistry, 2017, Vol. 90, No. 6, pp. 831−837. © Pleiades Publishing, Ltd., 2017.
Original Russian Text © N.A. Lomanova, M.V. Tomkovich, V.L. Ugolkov, V.V. Gusarov, 2017, published in Zhurnal Prikladnoi Khimii, 2017, Vol. 90, No. 6, pp. 673−679.

INORGANIC SYNTHESIS AND INDUSTRIAL INORGANIC CHEMISTRY

Formation and Thermal Properties of Nanocrystalline $Bi_4Ti_3O_{12}$

N. A. Lomanova[a]*, M. V. Tomkovich[a], V. L. Ugolkov[b], and V. V. Gusarov[a]

[a] *Ioffe Institute, ul. Politechnicheskaya 26, St. Petersburg, 194021 Russia*
**e-mail: natus@mail.ioffe.ru*
[b] *Grebenshchikov Institute of Silicate Chemistry, Russian Academy of Sciences, ul. Tiflisskaya 3/6, St. Petersburg, 199034 Russia*

Received July 28, 2017

Abstract—Mechanism by which nanocrystalline $Bi_4Ti_3O_{12}$ is formed in thermal treatment of coprecipitated hydroxides was studied. It was shown that the onset of the active formation is correlated with the melting point of the surface phase based on bismuth oxide. The technological synthesis parameters of $Bi_4Ti_3O_{12}$, at which crystallite sizes in the range 35–60 nm are provided, were determined.

DOI: 10.1134/S1070427217060015

Layered perovskite-like oxides of the type of the Aurrivillius phases [1] with general formula $A_{m-1}Bi_2B_mO_{3m+3}$ (A = Bi; B = Ti, Fe) are used in various fields of technology [2–6]. Bismuth titanate ($Bi_4Ti_3O_{12}$) is the end component of the homological series of the Aurrivillius phases $A_{m-1}Bi_2B_mO_{3m+3}$ [1] with $m = 3$ and has at room temperature a rhombic unit cell (space group Fmmm) in which three perovskite-like blocks $\{(Bi_4Ti_3O_{10})^{2-}\}$ alternate with fluorite-like layers $\{(Bi_2O_2)^{2+}\}$.

It is known that $Bi_4Ti_3O_{12}$ possesses piezoelectric [5], ferroelectric [6–8], and catalytic [9, 10] properties. This material has the following advantages in application: high values of the Curie point ($T_C \approx 675$°C), spontaneous polarization (50 μC cm^{-2}), and permittivity and also the lead-free composition. The technologies of non-volatile ferroelectric memory (FeRAM and NVRAM) based on perovskite-like materials, including Bi_4Ti_3O12, are being actively developed [7, 8].

According to the phase equilibrium data for the Bi_2O_3–TiO_2 system [11, 12], $Bi_4Ti_3O_{12}$ is stable up to 1200°C and melts with decomposition into a compound with pyrochlore structure (Bi_2Ti_2O7) above this temperature. At a temperature of about 1210°C $Bi_2Ti_4O_7$ decomposes to give the compound $Bi_2Ti_4O_{11}$, which, in turn, decomposes at 1240°C into titanium dioxide coexistent with the melt.

The formation mechanism and properties of macrocrystalline materials based on the Aurrivillius phases $A_{m-1}Bi_2B_mO_{3m+3}$ with varied number m of layers were considered in [13–20].It was shown that the rate determining process in the formation of these compounds is the mass transfer of the components into the reaction zone. Under the given conditions, a single-phase material is formed at temperatures higher than 800°C. It was shown in [13] that the specific feature of the solid-phase reaction yielding $Bi_4Ti_3O_{12}$, which consists in that the solid-phase interaction occurs simultaneously with the sintering and particle-growth processes, leads to a slower synthesis of the compound and to a possible deterioration of the functional properties of ceramic materials on its basis. It would be expected that the rate of $Bi_4Ti_3O_{12}$ formation can be raised and materials with single-phase composition and properties be obtained if the particles of reagents and reaction products are made smaller, including nanometer values, and their contact area is enlarged [21].

$Bi_4Ti_3O_{12}$ nanoparticles can be obtained under hydrothermal conditions [22, 23], by coprecipitation from

solutions [24–27], and by the sol-gel method [28, 29]. Despite that all the above methods of "soft chemistry" shift the crystallization onset of this compound to lower temperatures, obtaining a single-phase materials meets a number of difficulties in all cases. This is due to the appearance of impurity phases with close temperature ranges of formation in the reaction formulation based on the Bi_2O_3–TiO_2 system. To these phases belong $Bi_2Ti_2O_4$ (pyrochlore structure) and $Bi_{12}TiO_{20}$ (sillenite structure) compounds [24, 25]. Therefore, a search for effective technological modes for obtaining a nanocrystalline material based on $Bi_4Ti_3O_{12}$ is of particular interest [30]. The goal of our study was to synthesize $Bi_4Ti_3O_{12}$ via thermal decomposition of coprecipitated hydroxide and determine the optimal formation conditions and thermal properties of the nanocrystalline material based on this compound.

EXPERIMENTAL

Bismuth titanate $Bi_4Ti_3O_{12}$ was synthesized via thermal treatment of a mixture produced by coprecipitation from a solution of bismuth nitrate pentahydrate $Bi(NO_3)_3 \cdot 5H_2O$ (pure) and titanium isopropoxide $C_{12}H_{28}O_4Ti$ (97%) salts in 25% aqueous NH_4OH. Preliminarily, bismuth nitrate was dissolved in dilute nitric acid with concentration of 0.1 M (pH < 2). Titanium isopropoxide was dissolved in ethanol to preclude premature hydrolysis and added under permanent agitation to a bismuth nitrate solution in an amount corresponding to the $Bi_4Ti_3O_{12}$ stoichiometry. The thus prepared transparent solution was slowly poured under agitation into the ammonia solution, with pH > 8 maintained.

The coprecipitated mixture was washed on a filter with distilled water. The precipitate was dried at a temperature of about 80°C for 5 h. Then a sample was thermally treated at 350–800°C in the heating–isothermal keeping–cooling mode.

The microstructure and elemental composition of the samples were determined by scanning electron microscopy (SEM) and energy-dispersive microanalysis (FEI Quanta 200 scanning electron microscope with EDAX attachment) before and after their thermal treatment.

The phase state of the samples was determined by X-ray diffraction analysis Shimadzu XRD-7000 diffractometer CuK_α radiation, λ = 15.40598 nm). The unit cell parameters were calculated with PDWin 4.0 software package. The crystallite sizes were found from the widths of X-ray diffraction lines with the use of the Scherrer formula.

The thermal behavior was examined by synchronous thermal analysis including the differential scanning calorimetry (DSC) and thermogravimetry (TG) on a Netzsch STA 429 analyzer in air in the temperature range 40–1230°C at a heating rate of 5 deg min^{-1}.

The change in the linear dimension of a sample was determined with a Netzsch DIL 402 E dilatometer in air at a heating rate of 10 deg min^{-1} and a sample in the form of a pellet 5 mm in diameter and 3 mm thick, preliminarily sintered at 450°C.

RESULTS AND DISCUSSION

The method of coprecipitation of hydroxides from a solution of salts yielded a nanocrystalline powder in which the Bi : Ti elements ratio corresponds, according to the results of an elemental analysis, to stoichiometry to within the error of this technique. A nanocrystalline material based on bismuth titanate was produced by thermal decomposition of the precipitate. The results of an X-ray diffraction and synchronous thermal analyses made it possible to understand how this material is formed.

Figure 1 shows X-ray diffraction data for samples after different stages of their thermal treatment. The X-ray diffraction patterns of the coprecipitated mixture and a sample thermally treated at 350 and 400°C for 1 h show only an X-ray-amorphous substance (Fig. 1). As the temperature is raised to 450°C, the fraction of the X-ray-amorphous phase decreases, and there appear reflections corresponding to a crystalline phase based on $Bi_4Ti_3O_{12}$. According to [30], the intensification of the formation of perovskite-like bismuth-containing phases under "soft chemistry" conditions at 450 ± 50°C is associated with the transition of the surface of Bi_2O_3 particles to a liquid-like state, which activates the mass transfer in the reaction system.

To analyze phase changes in a sample at the onset temperature of its formation, it was thermally treated at 450°C, with isothermal keeping for 1, 3, 5, and 10 h. The corresponding X-ray diffraction patterns are shown in Fig. 2a. These results indicate that the thermal treatment duration strongly affects the phase changes occurring in a sample. The substantial amount of the X-ray-amorphous phase, observed upon a thermal treatment for 1 h, markedly decreases as the keeping duration is raised to 3 h

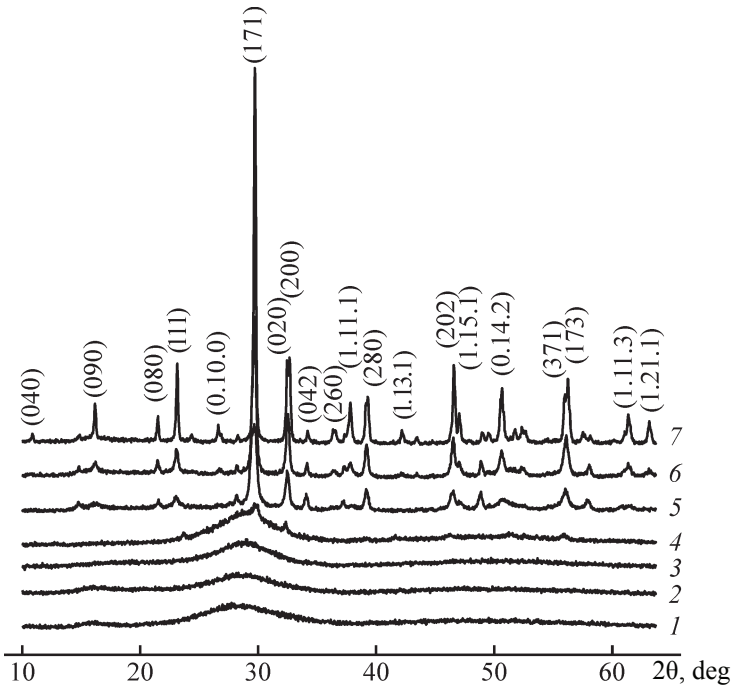

Fig. 1. (*1*) X-ray diffraction pattern of coprecipitated mixture at 25°C and diffraction patterns upon its thermal treatment for 1 h at temperatures of (*2*) 350, (*3*) 400, (*4*) 450, (*5*) 500, (*6*) 600, and (*7*) 800°C.

and more. At the same time, the average size of $Bi_4Ti_3O_{12}$ crystallites is independent of the thermal treatment duration and remains on the same level (Fig. 2b).

For a sample subjected to successive thermal treatments (Fig. 1), a sharp decrease in the fraction of the X-ray amorphous phase is observed after the isothermal keeping at 500°C for 1 h (Figs. 2 and 3a). The fact that the content of the X-ray-amorphous phase in a sample decreases without appearance of other crystalline phases in the reaction system shows that it is fully consumed for the formation ob $Bi_4Ti_3O_{12}$ nanocrystals. The thermal treatment of a sample at 500–800°C does not lead to noticeable changes of the phased state as compared with a sample subjected to a thermal treatment at 500°C. It should be noted that the X-ray diffraction patterns of a sample subjected to a thermal treatment below 800°C show no reflection splitting (0.12.0)/(200), (371)/(173) characteristic of the rhombic modification of $Bi_4Ti_3O_{12}$. The insufficient precision of the X-ray measurements made in this experiment gives no way of accurately characterizing the structure of the substance formed under the conditions described above, but suggests that a phase with a higher crystal-lattice symmetry is formed in the initial stage of the synthesis. This possibility was noted in [20, 125, 28] where the formation of a tetragonal modification of $Bi_4Ti_3O_{12}$ was observed at temperatures

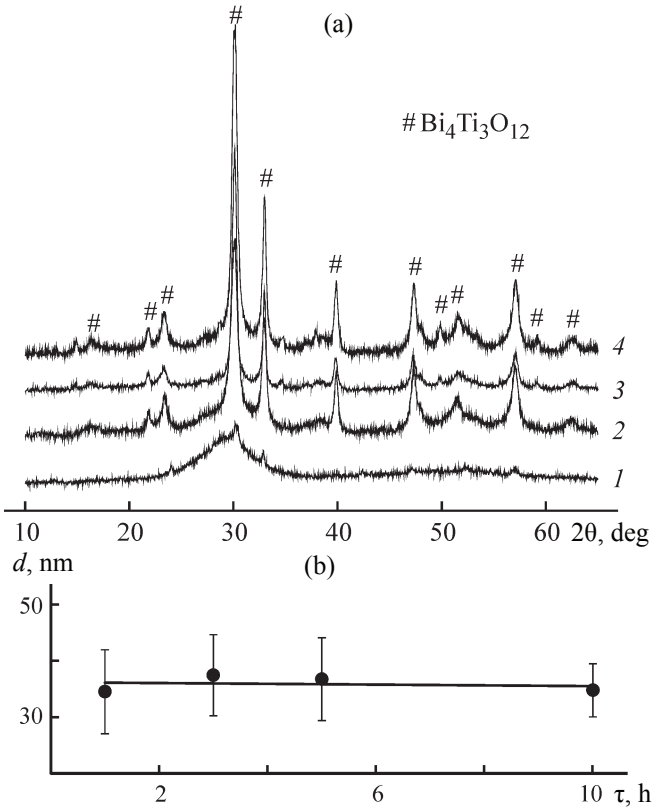

Fig. 2. (a) X-ray diffraction patterns of a sample thermally treated at 450°C for (*1*) 1, (*2*) 3, (*3*) 5, and (*4*) 10 h and (b) dependence of the average $Bi_4Ti_3O_{12}$ crystallite size *d* on thermal treatment duration τ.

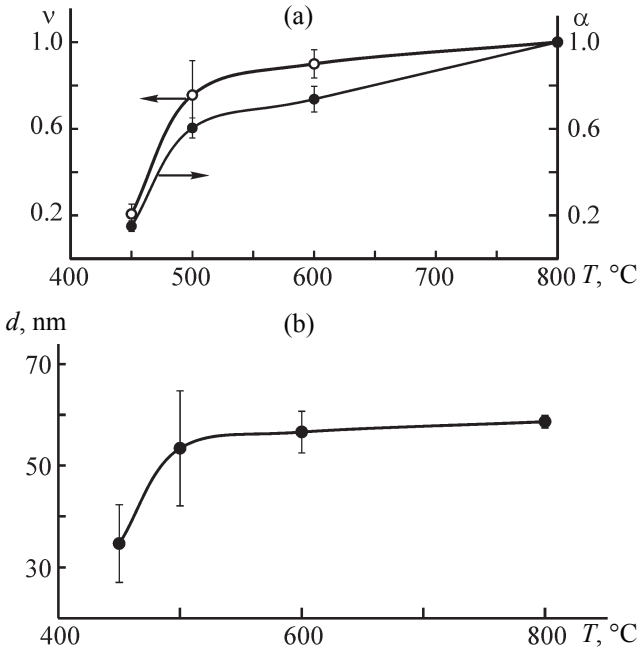

Fig. 3. Variation of (a) volume fraction v and conversion α and (b) crystallite size d of $Bi_4Ti_3O_{12}$ with increasing temperature T.

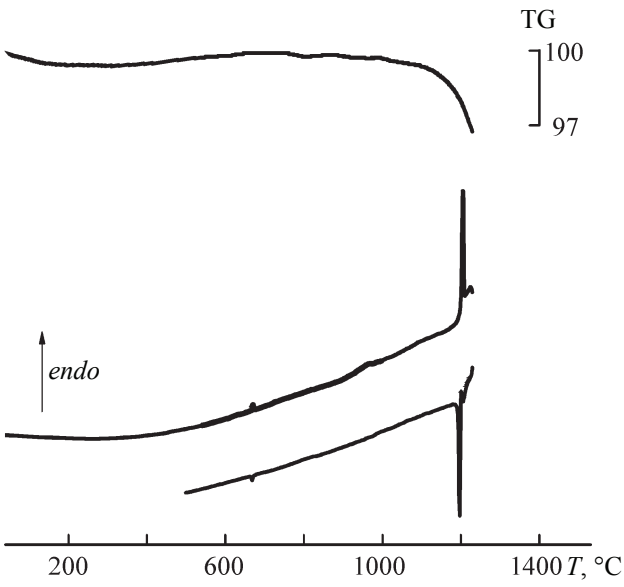

Fig. 4. Thermal analysis (DSC/TG) of a $Bi_4Ti_3O_{12}$ sample. (T) Temperature; the same for Fig. 5.

of up to 750°C. The unit cell parameters and the X-ray density of $Bi_4Ti_3O_{12}$ in different stages of thermal treatment are presented in the table.

Figure 4 presents the results of a synchronous thermal analysis, which make it possible to analyze the thermal behavior of the nanocrystalline $Bi_4Ti_3O_{12}$ we obtained. At temperatures below 600°C, DSC/TG curves show no significant thermal transformations. A small endothermic peak is observed at a temperature of 665 ± 5°C, which corresponds to a second-order phase transition (Curie point) in $Bi_4Ti_3O_{12}$ [10]. A small loss of mass (~3%) by a sample is observed above 900°C. A strong endothermic peak is observed in the DSC curve, together with a considerable loss of mass, at 1190 ± 5°C, and corresponds to the decomposition onset of $Bi_4Ti_3O_{12}$. This peak is imposed by a weak endothermic effect at 1210°C, which is presumably associated with the decomposition of $Bi_2Ti_2O_7$ that is formed in destruction of $Bi_4Ti_3O_{12}$. These peaks are repeated in the cooling curve in the reverse order at somewhat different temperatures, which is accounted for y kinetic effects. The appearance of a liquid phase in the decomposition of $Bi_4Ti_3O_{12}$ is accompanied by a sharp increase in the loss of mass by a sample, which is presumably due to the high volatility of Bi_2O_3 in the liquid state. The data we obtained demonstrate that the thermal behavior of the $Bi_4Ti_3O_{12}$ compound in the form of a nanocrystalline substance is similar to its behavior in the macrocrystalline state, described in [14].

To determine the optimal synthesis temperature of the nanocrystalline bismuth titanate, we analyzed the dependences that reflect the phase formation in the system in successive heatings of a sample for 1 h and the corresponding changes in the crystallite size (Fig. 3). It is noteworthy that the smallest crystallite size is observed in the case of a thermal treatment at 450°C, when the formation of $Bi_4Ti_3O_{12}$ is activated. A prolonged thermal treatment of a sample at this temperature hardly changes the size of the crystallites (Fig. 2b). The subsequent thermal treatment of the sample at 500°C and higher temperatures leads to a sharp increase in the crystallite size. Upon a calcination of the samples in the temperature range 500–800°C, the crystallite size reaches a value of 50–60 nm and remains on approximately the same level, irrespective of the calcination temperature (Fig. 3b).

Comparison of the data on how the relative average volume of the crystallites, $v = (d/d_{max})^3$, and the fraction of nanocrystalline $Bi_4Ti_3O_{12}$ grow with increasing thermal-treatment temperature shows that these values coincide within the measurement error. This indicates that, in the case of a thermal treatment at 50°C and above, the formation mechanism of bismuth titanate is determined by the growth of nanocrystals due to the crystallization of the X-ray-amorphous substance on these nanocrystals. At the same time, the data on how the content of the crystalline phase changes at different durations of the thermal treat-

Characteristics of $Bi_4Ti_3O_{12}$

T, °C	Crystallographic system	a	b	c	ρ, g cm^{-3}	$\alpha_t \times 10^{-6}$, K^{-1}	T_s, °C
		Å					
–	Tetragonal	3.86 [20]		32.65 [20]	–	8.5 [31] 11.0 ± 1.0 [19]	720 [19]
450		3.86		31.76	8.2	7.2 ± 2.0	680
500		3.85		31.73	8.2		
600		3.85		31.75	8.2		
800	Rhombic	5.42	5.41	32.71	8.1	–	
–		5.45[a]	5.41[a]	32.82[a]	–		

[a] Data of the X-ray data base PDWin 4.0 (N 35-795).

ment at 450°C show, with consideration for the unchanging crystallite size, that the key role in the formation of nanocrystalline $Bi_4Ti_3O_{12}$ at this temperature is played by the nucleation process. Thus, the phase-formation mechanism changes from dominance of the nucleation process to that of particle growth lies in the case under consideration in the temperature range 450–500°C.

The results we obtained suggest the following scheme of controlling the size of $Bi_4Ti_3O_{12}$ crystallites in their synthesis by thermal decomposition of coprecipitated hydroxides. By changing the duration of a thermal treatment at 450°C, we can vary the relative amounts of $Bi_4Ti_3O_{12}$ nanocrystals and X-ray-amorphous phase. It is possible in principle to produce by a prolonged thermal treatment at 4550°C a 100% yield of the target product with crystallite size of about 35 nm. In turn, the ratio between the crystalline and X-ray-amorphous phases determines the size of $Bi_4Ti_3O_{12}$ crystallites in thermal treatment of the mixture at 500°C and more, when the process in which $Bi_4Ti_3O_{12}$ crystallites grow is predominant. Consequently, it is possible to obtain bismuth titanate with crystallite size of 35–60 nm via this double-stage annealing by varying the duration of calcination at 450 and 500°C.

The dilatometric method was used to analyze in the temperature range 200–800°C the behavior of the nanocrystalline $Bi_4Ti_3O_{12}$ powder produced by thermal treatment at 450°C. The dilatometric curve shown in Fig. 5 demonstrates that a sample strongly shrinks at the temperature T_s = 680 ± 5°C, found from the peak in the $\Delta L/L_0(T)$ curve, which is due to the intensified gain-to-grain sintering. The average linear thermal expansion coefficient of nanocrystalline $Bi_4Ti_3O_{12}$, found in the range 450–600°C in which no noticeable phase transformations occur, id $\alpha_t = 7.2 \pm 2.0 \times 10^{-6}$ K^{-1} (see the table).

The sintering of the resulting material is illustrated by SEM data for different synthesis stages. Figure 6 shows SEM images of the powder after its successive thermal treatments at temperatures of 450 and 800°C. The starting formulation is constituted by agglomerates of particles. SEM images show that, with increasing temperature, the agglomerates are sintered together to form grains with more distinct boundaries and size of 0.5 ± 0.1 μm (Fig. 6). Thus, not only the size of $Bi_4Ti_3O_{12}$ crystallites, but also the process of sintering and growth of grains in

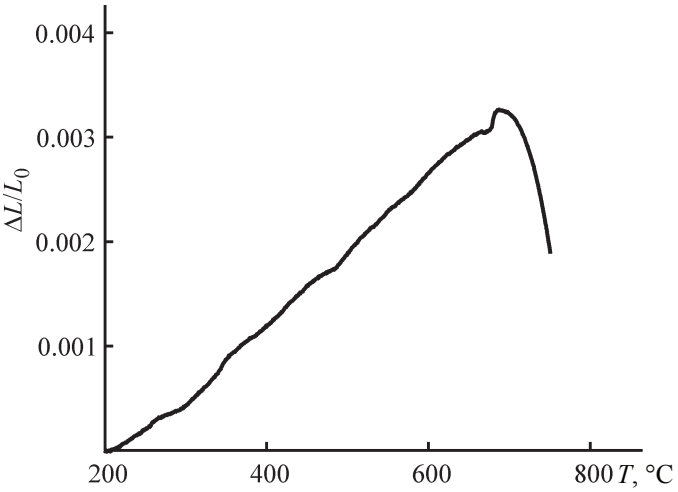

Fig. 5. Dilatometric analysis of nanocrystalline $Bi_4Ti_3O_{12}$.

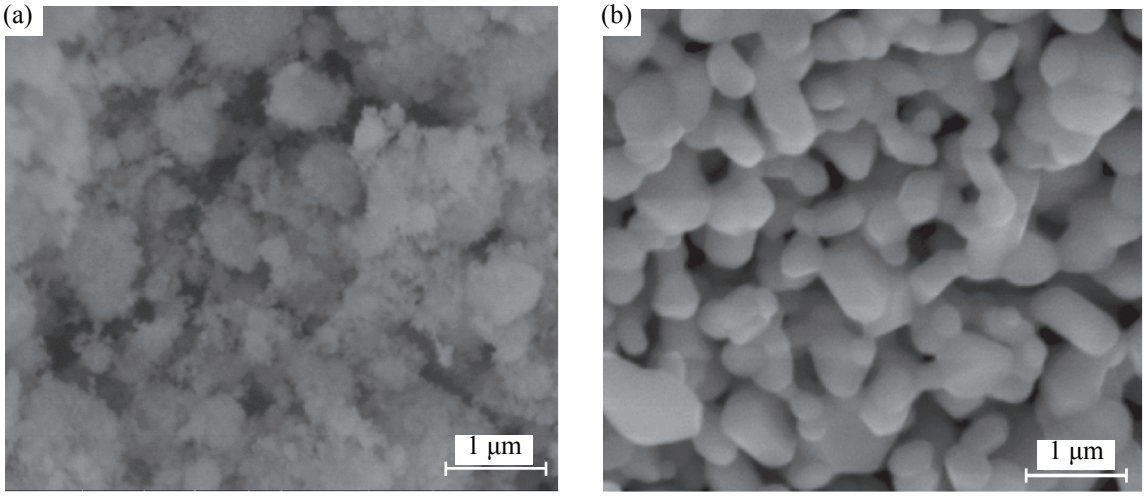

Fig. 6. SEM images of a $Bi_4Ti_3O_{12}$ sample upon its thermal treatment at (a) 450 and (b) 800°C.

the ceramic material can be controlled by varying the calcination temperature within the range 450–800°C and the thermal treatment duration.

CONCLUSIONS

The process is described in which a nanocrystalline material based on $Bi_4Ti_3O_{12}$ is formed in thermal treatment of coprecipitated hydroxides. It was shown that formation of $Bi_4Ti_3O_{12}$ nanocrystals is initiated at a temperature of about 450°C, which is correlated with the melting onset of the surface phase based on bismuth oxide. It was found that the growth of crystallites becomes the dominant process at temperatures higher than 500°C. This process is slowed down after the crystallization of the X-ray-amorphous phase. The temperatures of the second-order phase transition, sintering activation, and decomposition onset of te material based on nanocrystalline bismuth titanate. It is shown that the intense sintering of nanocrystalline $Bi_4Ti_3O_{12}$ occurs in the range 700–800°C and is manifested in densification of agglomerates of $Bi_4Ti_3O_{12}$ nanoparticles.

ACKNOWLEDGMENTS

The study was supported by the Russian Science Foundation (project no. 16-13-10252).

REFERENCES

1. Aurrivillius, B., *Ark. Kemi*, 1949, vol. 1, no. 1, pp. 463–471.
2. Keeney, L., Maity, T., Schmidt, M., et al., *J. Am. Ceram. Soc.*, 2013, vol. 96, pp. 2339–2357.
3. Jiang, P.P., Zhang, X.L., Chang, P., et al., *J. Appl. Phys.*, 2014, vol. 115, pp. 144101–144105.
4. Birenbaum, A.Y. and Ederer, C., *Phys. Rev. B*, 2014, vol. 90, pp. 214109–214112.
5. Long, C., Chang, Q., and Fan, H., *Sci. Rep.*, 2017, vol. 7, no. 1, pp. 4193–4215.
6. Bartkowska, J.A., Dercz, J., and Michalik, D., *Sol. St. Phenom.*, 2015, vol. 226, pp. 17–22.
7. Chen, K.-H., Diao, C.-C., Yang, C.-F., and Wang, B.-X., *Ferroelectr.*, 2009, vol. 385, pp. 46–53.
8. Kalinkin, A.N., Kozhbakhteev, E.M., Polyakov, A.E., and Sborikov, V.M., *Inorg. Mater.*, 2013, vol. 49, no. 10, pp. 1031–1043.
9. Wei, W., Dai, Y., and Huang, B., *J. Phys. Chem. C*, 2009, vol. 113, no. 14, pp. 5658–5663.
10. Cui, Z.M., Yang, H., Zhang, M., et al., *Mater. Trans.*, 2016, vol. 57, no. 10, pp. 1766–1770.
11. Kargin, Yu.F., Ivicheva, S.N., and Volkov, V.V., *Russ. J. Inorg. Chem.*, 2015, vol. 60, no. 5, pp. 619–625.
12. Esquivel-Elizondo, J.R., Hinojosa, B.B., and Nino, J.C., *Chem. Mater.*, 2011, vol. 23, pp. 4965–4974.
13. Morozov, M.I., Mezentseva, L.P., and Gusarov, V.V., *Russ. J. Gen. Chem.*, 2002, vol. 72, no. 7, pp. 1110–1113.
14. Lomanova, N.A., Morozov, M.I., Ugolkov, V.L., and Gusarov, V.V., *Inorg. Mater.*, 2006, vol. 42, no. 2, pp. 189–195.
15. Navarro-Rojero, M.G., Romero, J.J., Rubio-Marcos, F., and Fernandez, J.F., *Ceram. Int.*, 2010, vol. 36, pp. 1319–1325.
16. Lomanova, N.A., Semenov, V.G., Panchuk, V.V., and Gusarov, V.V., *J. Alloys Compd.*, 2012, vol. 528, pp. 103–108.

17. Lomanova, N.A., Ugolkov, V.L., Panchuk, V.V., and Semenov, V.G., *Russ. J. Gen. Chem*., 2017, vol. 87, pp. 365–372.
18. Gumiel, C., Bernardo, M.S., Villanueva, P.G., et al., *J. Mater. Sci*., 2017, vol. 52, pp. 4042–4051.
19. Wong, Y.J, Hassan, J., Chen, S.K., and Ismail, I., *J. Alloys Compd*., 2017, vol. 723, pp. 567–579.
20. Stojanovic, B.D., Paiva-Santos, C.O., Cilense, M., et al., *Mater. Res. Bull*., 2008, vol. 43, pp. 1743–1753.
21. Gusarov, V.V., *Russ. J. Gen. Chem*., 1997, vol. 67, no. 12, pp. 1846–1851.
22. Xu, G., Yang, Y., Bai, H., et al., *Cryst. Eng. Comm.,* 2016, vol. 18, no. 13, pp. 2268–2274.
23. Gu, H., Hu, Z., Hu, Y., et al., *Colloids Surf. A*, 2008, vol. 315, nos. 1–3, pp. 294–298.
24. Kana, Y., Wang, P., Li, Y., et al., *Mater. Lett.,* 2002, vol. 56, pp. 910–914.
25. Lisoni ,J.G., Millan, P., Vila, E., et al., *Chem. Mater.,* 2001, vol. 13, pp. 2084–2091.
26. Zhang, F., Karaki, T., and Adachi, M., *Jap. J. Appl. Phys.,* 2006, vol. 45, no. 9B, pp. 7385–7388.
27. Chen Zhihui, Qiu Junfu, Liu Cheng, et al., *Ceram. Int.,* 2010, vol. 36, pp. 241–244.
28. Kidcho, T., Malfatti, L., Marongiu, D., et al., *J. Am. Ceram. Soc.,* 2010, vol. 93, no. 9, pp. 2897–2902.
29. Ma, C.H., Lin, X., Wang, L., and Yan, Y.S., *Adv. Mater. Res.,* 2014, vol. 997, pp. 359–362.
30. Lomanova, N.A. and Gusarov, V.V., *Russ. J. Gen. Chem.,* 2013, vol. 83, no. 12, pp. 2251–2253.
31. Kato, T., *Jap. J. Appl. Phys.,* 1983, vol. 22, pp. 47–49.